The environment and characteristics of low redshift galaxies detected by the *Herschel*-ATLAS

A. Dariush[1,20]★ , L. Cortese[13], S. Eales[1], E. Pascale[1], M. W. L. Smith[1], L. Dunne[2],
S. Dye[1,2], D. Scott[30], R. Auld[1], M. Baes[6], J. Bland-Hawthorn[31],S. Buttiglione[9], A. Cava[3],
D.L. Clements[20], A. Cooray[21],G. DeZotti[9,26], S. Driver[11], J. Fritz[6], H.L. Gomez[1], A. Hopkins[12],
R. Hopwood[20],R.J. Ivison[7,14], M.J. Jarvis[22,29], D.H. Jones[12], L. Kelvin[11], H. G. Khosroshahi[32],
J. Liske[13], J. Loveday[15], S. Maddox[2], B.F. Madore[28], M.J. Michałowski[14], P. Norberg[14],
S. Phillipps[4], M. Pohlen[1], C.C. Popescu[18], A.S.G. Robotham[11], G. Rodighiero[27], M. Prescott[10],
E. Rigby[2], M. Seibert[28], D.J.B. Smith[2], P. Temi[8], R.J. Tuffs[19], P. van der Werf[14,23]

[1]*School of Physics and Astronomy, Cardiff University, the Parade, Cardiff, CF24 3AA, UK*
[2]*School of Physics and Astronomy, University of Nottingham, University Park, Nottingham NG7 2RD, UK*
[3]*Departamento de Astrofísica, Facultad de CC. Físicas, Universidad Complutense de Madrid, E-28040 Madrid, Spain*
[4]*Astrophysics Group, H.H. Wills Physics Laboratory, University of Bristol, Tyndall Avenue, Bristol BS8 1TL, UK*
[5]*Laboratoire dAstrophysique de Marseille, UMR6110 CNRS, 38 rue F. Joliot-Curie, F-13388 Marseille France*
[6]*Sterrenkundig Observatorium, Universiteit Gent, Krijgslaan 281 S9, B-9000 Gent, Belgium*
[7]*UK Astronomy Technology Centre, Royal Observatory, Edinburgh, EH9 3HJ, UK*
[8]*Astrophysics Branch, NASA Ames Research Center, Mail Stop 245-6, Moffett Field, CA 94035, USA*
[9]*INAF Osservatorio Astronomico di Padova, Vicolo Osservatorio 5, I-35122, Padova, Italy*
[10]*Astrophysics Research Institute, Liverpool John Moores University, 12 Quays House, Egerton Wharf, Birkenhead, CH41 1LD, UK*
[11]*SUPA, School of Physics and Astronomy, University of St. Andrews, North Haugh, St. Andrews, KY16 9SS, UK*
[12]*Australian Astronomical Observatory, PO Box 296, Epping, NSW, 1710, Australia*
[13]*European Southern Observatory, Karl-Schwarzschild-Strasse 2 D-85748, Garching bei Munchen, Germany*
[14]*SUPA, Institute for Astronomy, University of Edinburgh, Royal Observatory, Blackford Hill, Edinburgh EH9 3HJ, UK*
[15]*Astronomy Centre, Department of Physics and Astronomy, University of Sussex, Falmer, Brighton, BN1 9QH, UK*
[18]*Jeremiah Horrocks Institute, University of Central Lancashire, Preston, PR1 2HE, UK*
[19]*Max-Planck-Institut für Kernphysik, Saupfercheckweg 1, D-69117, Heidelberg, Germany*
[20]*Physics Department, Imperial College London, Prince Consort Road, London, SW7 2AZ, UK*
[21]*Department of Physics and Astronomy, UC Irvine, Irvine, CA 92697, USA*
[22]*Centre for Astrophysics Research, Science & Technology Research Institute, University of Hertfordshire, Hatfield, Herts, AL10 9AB, UK*
[23]*Leiden Observatory, Leiden University, PO Box 9513, NL - 2300 RA Leiden, The Netherlands*
[24]*International Centre for Radio Astronomy Research, The University of Western Australia, 35 Stirling Hwy, Crawley, WA 6009, Australia*
[26]*SISSA, Via Bonomea 265, I-34136 Trieste, Italy*
[27]*University of Padova, Vicolo Osservatorio 3, I-35122 Padova, Italy*
[28]*Observatories of the Carnegie Institution of Washington, 813 Santa Barbara Str, Pasadena, CA91101, USA*
[29] *Physics Department, University of the Western Cape, Cape Town, 7535, South Africa*
[30]*Department of Physics & Astronomy, University of British Columbia, 6224 Agricultural Road, Vancouver, BC, V6T1Z1, Canada*
[31]*Sydney Institute for Astronomy, University of Sydney, NSW 2006, Australia*
[32]*IPM School of Astronomy, Larak Garden, opposite Araj, Artesh Highway,Tehran, Iran*

1 July 2011

ABSTRACT

We investigate the ultraviolet and optical properties and environment of low redshift galaxies detected in the *Herschel* Astrophysical Terahertz Large Area Survey (H-ATLAS) science demonstration data. We use the Sloan Digital Sky Survey seventh release and the Galaxy And Mass Assembly database to select galaxies with $r_{\rm Petro} \leqslant 19.0$ mag in the redshift range $0.02 \leqslant z \leqslant 0.2$ and look for their submillimeter counterparts in H-ATLAS. Our results show that at low redshift, H-ATLAS detects mainly blue/star-forming galaxies with a minor contribution from red systems which are highly obscured by dust. In addition we find that the colour of a galaxy rather than the local density of its environment determines whether it is detectable by H-ATLAS. The average dust temperature of galaxies that are simultaneously detected by both PACS and SPIRE is 25 ± 4 K, independent of environment. This analysis

arXiv:1106.6195v1 [astro-ph.CO] 30 Jun 2011

1 INTRODUCTION

The wide range of observed physical characteristics of galaxies is indicative of a large variance in galaxy formation history. Observations show that the environment of a galaxy plays an important role in shaping its observed properties. Dressler (1980) showed that galaxy morphology is a strong function of galaxy density and numerous studies since then have demonstrated the dependence of galaxy properties on local environment (Lewis et al. 2002; Gomez et al. 2003; Balogh et al. 2004a,b; Blanton et al. 2005; Park et al. 2007; O'Mill, Padilla & Lambas 2008; Ball, Loveday & Brunner 2008; Lee et al. 2010).

Results from large sky surveys such as the Sloan Digital Sky Survey (SDSS) have revealed that the distribution of galaxy colours is bimodal, i.e., the so called 'blue cloud' versus the 'red sequence' (Strateva et al. 2001; Baldry et al. 2004). The relative numbers of blue and red galaxies at a fixed luminosity are observed to vary strongly with local density, with blue and red galaxies predominantly populating low and high density environments, respectively (e.g. Balogh et al. 2004b; Ball, Loveday & Brunner 2008). The major factors that influence the observed colour of a galaxy are its star formation history (SFH), the amount of dust attenuation, and metallicity (Johnson et al. 2006, 2007). The vast majority of galaxies in the blue cloud are actively forming stars while the red sequence consists mainly of early-type passive galaxies (i.e., having little or no current star formation) with additional minor contributions from heavily obscured star-forming galaxies or edge-on systems.

Analyses of the dust attenuation in star-forming galaxies suggest that in comparison to quiescent systems, star-forming objects are heavily affected by internal dust extinction (Wyder et al. 2007; Johnson et al. 2007; Driver et al. 2007; Cortese et al. 2008; Tojeiro et al. 2009). In such galaxies, UV radiation heats dust grains which then re-radiate at far-infrared (FIR) wavelengths. However, thermally emitting dust detected by, for example, *IRAS* (at $25 - 100\mu$m) can often only constitute a small fraction of a galaxy's total dust mass. Results from the SCUBA Local Universe Galaxy Survey (Dunne & Eales 2001; Vlahakis, Dunne & Eales 2005), as well as those of the sample of the Virgo cluster studied in Popescu et al. (2002) and Tuffs et al. (2002), using the ISOPHOT instrument on board the *Infrared Space Observatory* (*ISO*), show that there is a population of galaxies containing much larger proportions of cold dust that radiates at > 100 μm in submillimeter bands. As such, submillimeter observations provide invaluable information for estimating the total dust content of these galaxies which in turn helps us to understand relationships with other galaxy properties. For instance, although we know there is a clear division between the optical properties of galaxies on the red sequence and those in the blue cloud, we do not know if this is reflected in their submillimeter properties.

In the present study, we use submillimeter data acquired by the *Herschel* Space Observatory as a part of the *Herschel* Astrophysical Terahertz Large Area Survey (H-ATLAS; Eales et al. 2010). The H-ATLAS survey is an open-time programme to survey ~600 deg^2 of the extragalactic sky over the wavelength range 110–500 μm using the Photodetector Array Camera and Spectrometer (PACS; Poglitsch et al. 2006) and Spectral and Photometric Imaging REceiver (SPIRE; Griffin et al. 2010). H-ATLAS also covers the largest area in a blind extragalactic survey with *Herschel*. One of the aim if to provide the FIR equivalent for the SDSS and 2dFGRS (Two-degree Field Galaxy Redshift Survey; Colless et al. 2001) surveys is to characterize the properties of nearby galaxies. Also, for all regions covered by H-ATLAS, spectroscopic com-

pleteness will be guaranteed only up to the redshift of the GAMA survey [1](e.g. $z \lesssim 0.2$; Driver et al. 2010). So detailed statistical analysis will mainly be possible in the local universe. Therefore it is crucial to understand what kind of nearby galaxies are detected by H-ATLAS to provide a useful characterization of the FIR properties of local galaxies. In addition, we are also going to characterize the relationship between the nature and environment of submillimeter sources detected in H-ATLAS. So by concentrating on sources at low redshifts, we are able to have a better estimation of the galaxy projected density since such measurements become difficult at higher redshifts due to a decrease in the observed limiting luminosity of galaxies with spectroscopic redshifts. Also, nearby sources can be spatially resolved far more easily (e.g. less blending), so that we can see where the submillimeter emission is coming from, unlike for sources at high redshifts.

The submillimeter data analysed in this study were acquired during *Herschel*'s Science Demonstration Phase (SDP) and cover an area of ~ 14.5 deg^2. Three main advantages of *Herschel* over previous infrared observatories are its broad wavelength range, high sensitivity and high angular resolution. The wavelength range in particular encompasses the peak of the far-IR/submillimeter part of the spectral energy distribution for low redshift galaxies thus allowing accurate measurements of total dust mass. In contrast, other submillimeter surveys such as those conducted by the *Balloon-borne Large-Aperture Submillimeter Telescope* (*BLAST*) with observations at 250μm, 350μm, and 500μm, have lower angular resolution and do not cover more than ~20 deg^2 of the extragalactic sky (Pascale et al. 2008; Devlin et al. 2009).

The layout of this paper is as follows. In §2, we provide a summary of our submillimeter sample selection, optical photometric and spectroscopic observations from the SDSS/GAMA surveys, and UV observations from GAMA/*GALEX* survey (Seibert et al. 2010). A summary of the parameters estimated from our data is given in §3. Our final results and concluding remarks are given in §4.

2 DATA

We will use the SDSS DR7 (Abazajian et al. 2009) together with the Galaxy And Mass Assembly redshift survey (GAMA survey; Driver et al. 2010) to compile an optically selected sample of low-redshift galaxies, and from there, look at the optical properties of those sources detected by *Herschel*. Here, we summarize the data in each survey and describe our sample selection.

2.1 Optical/UV data

Optical sources used in this paper were initially taken from the SDSS DR7 (Abazajian et al. 2009). Our aim is to have an optically selected sample of galaxies with the criterion $0.02 \leqslant z \leqslant 0.2$. To do this, all SDSS sources from the GALAXY table were selected and their positions were cross-matched within 0.5 arcsec with objects from the GAMA survey in order to extract their spectroscopic redshifts as well as colours. The GAMA survey is based on data from SDSS DR6 and UKIDSS-LAS DR4 and consists of three equatorial regions named GAMA-09h, GAMA-12h, and GAMA-15h. The field observed by *Herschel*, coincides with the GAMA-09h equatorial region

---

[1] A detailed description of the GAMA survey is given in Sec.2.1

(Ra $= 129.0, 141.0$ deg; Dec $= -1.0, +3.0$ deg) where its spectroscopic survey is complete up to Petrosian magnitude, $r \lesssim 19.4$ (Robotham et al. 2010). Moreover, the GAMA data contains r-band defined aperture matched photometry in FUV/NUV (far-ultraviolet/near-ultraviolet) from *GALEX* and in *ugriz* optical bands from SDSS (Hill et al. 2011). We only select objects with the GAMA spectroscopic redshift quality parameter $Q \geqslant 3$, which approves their inclusion in scientific analysis (Driver et al. 2010). In our optical sample, $\sim$1.4 per cent of sources with $0.02 \leqslant z \leqslant 0.2$ have $Q < 3$.

We find a total of ~ 3370 galaxies in the redshift range $0.02 \leqslant z \leqslant 0.2$ within $\approx$12.5 deg^2 of our $\approx$14.5 deg^2 SDP field. The coverage is not complete, because the GAMA data goes down to Dec $= -1.0$ deg. In addition to optical fluxes, NUV magnitudes were available for ~ 2680 galaxies (Seibert et al. 2010; Hill et al. 2011). All magnitudes are corrected for Galactic extinction.

2.2 Submillimeter data

The H-ATLAS SDP data were acquired in November 2009 using *Herschel*'s parallel/fast scan mode, scanning at 60 arcsec s^{-1}. In this mode, mapping by PACS at 100 and 160 μm and SPIRE at 250, 350, and 500μm were carried out simultaneously. The SDP data covers an area of ~ 4.0 deg $\times$ 3.6 deg centered on $(\alpha, \delta) \approx$ $(09^{\rm h}05^{\rm m}, +0°30')$.

A complete description of the data reduction and noise analysis of PACS and SPIRE data are given in Ibar et al. (2010) and Pascale et al. (2010), respectively. Observed time-line data from both instruments were processed by using the *Herschel* Interactive Processing Environment (HIPE) using custom reduction scripts. Thermal drift in bolometer arrays was corrected by applying high-pass filtering. The naive map-making method of HIPE was used to project the two cross-scan timeline observations.

The estimated point spread functions (PSFs) of the final maps have full width at half maximum (FWHM) values of 8.7, 13.1, 18.1, 25.2, and 36.6 arcsec at 100, 160, 250, 350 and 500 μm, respectively. The estimated 1σ noise levels at 100, 160, 250, 350, and 500μm are 25–30, 33–48, 6.6 , 7.6, and 9.0 mJy/beam, respectively (Ibar et al. 2010; Rigby et al. 2010).

Sources were extracted using the 250 μm map as described in Rigby et al. (2010). The typical positional error for a $\geqslant$5 σ source is 2.5 arcsec or less. For each 250 μm source, corresponding 350 and 500 μm flux densities were measured by using the noise-weighted/beam-convolved 350 and 500 μm maps at the source position determined from the 250 μm map. Fluxes at 100 and 160 μm were estimated by matching each 250 μm source to the nearest PACS sources within a radius of 10 arcsec.

2.2.1 The submillimeter source catalogue

The H-ATLAS standard source catalogue of Rigby et al. (2010) is supplemented with cross-identification information from GAMA and SDSS DR7 surveys as described in Smith et al. (2010). A likelihood-ratio analysis (Sutherland & Saunders 1992) is performed by Smith et al. (2010) to match 250μm sources to SDSS DR7 sources brighter than $r=22.4$ mag. The probability that an optical source is in fact associated with the submillimeter source has been used to define the `Reliability` parameter. According to Smith et al. (2010), objects with `Reliability`$\geqslant$ 0.8 are considered to be true matches to submillimeter sources.

While we use the SDSS galaxy IDs to obtain the H-ATLAS

PACS and SPIRE submillimeter fluxes, we apply the same reliability cut as suggested by Smith et al. (2010), i.e. `Reliability`$\geqslant$ 0.8 which guarantees that we are $\sim$93 per cent ($\sim$ 83 per cent) complete in the redshift range $0.02 \leqslant z \leqslant 0.1$ ($0.1 < z \leqslant 0.2$). As such, throughout this paper, we refer to a 'detected source' as an SDSS galaxy with a $\geqslant 5.0\sigma$ submillimeter counterpart that has `Reliability`$\geqslant$ 0.8. Accordingly, we detect 496 galaxies at 250μm of which 482 ($\sim$ 97.2 per cent) have associated NUV fluxes. Thus in 14 galaxies ($\lesssim$ 2.8 per cent) with submillimeter detections we found no UV counterpart, but this will not affect the main results of the paper.

3 ANALYSIS

3.1 Summary of source detection

The first step of our analysis is to determine the rate of source detection in H-ATLAS as a function of galaxy r-band magnitude. The r-band magnitude is useful since it can be used as a starting point in sample selection for other extragalactic studies of low redshift galaxies using the *Herschel* submillimeter data. To do so, for all galaxies, we plot $(u - r)$ vs. Petrosian magnitude $r_{\rm Petro}$ corrected for Galactic extinction [2].

As Fig. 1 shows, the overall distribution of galaxies (gray contour lines) in $u - r$ colour is bimodal, showing blue cloud and red sequence galaxies. The overlaid data points represent galaxies with submillimeter detections made by SPIRE (left panel) and PACS (right panel). Horizontal and vertical histograms in each panel show the distribution of data points corresponding to individual SPIRE/PACS bands along the magnitude and colour axes, respectively.

Fig. 1 shows that the majority of galaxies with submillimeter detections are located in the blue cloud, with histograms of their colour peak around $u - r \approx 1.4$ without substantial red tails. Thus, within the redshift slice of the current sample of galaxies, the survey on the whole is mapping the blue sequence. Furthermore, a comparison between histograms at 250 μm and those in other SPIRE/PACS bands show that the SPIRE 250 μm band is by far the most sensitive, since the estimated rate of detections are higher at 250μm compared to other submillimeter bands. This is due to the higher sensitivity of SPIRE over PACS as well as the higher resolution of the 250μm map. With this in mind, in the analysis that follows, we only consider sources with 250 μm detections.

The quantities plotted in Fig. 1 are also shown in Fig. 2, but as a function of absolute r-band magnitude M_r and for sources with 250 μm detections. 'Left' and 'right' panels correspond to redshift bins $0.02 \leqslant z \leqslant 0.1$ and $0.1 \leqslant z \leqslant 0.2$, respectively. The absolute magnitude M_r is given by

$$M_r = r_{\rm Petro} - k_r - 5\log\left(\frac{D_{\rm L}}{10{\rm pc}}\right), \qquad (1)$$

where $D_{\rm L}$ is the luminosity distance, and k_r is the k-correction using the method of Chilingarian, Melchior & Zolotukhin (2010).

---

[2] The SDSS Petrosian magnitude is a modified form of the Petrosian (1976) system in which galaxy fluxes are measured within a circular aperture $\mathcal{R}_{\rm P}$(Petrosian radius) such that the ratio of the local surface brightness in an annulus at $\mathcal{R}_{\rm P}$ to the mean surface brightness within $\mathcal{R}_{\rm P}$, is equal to some constant value. Alternatively we can use the SDSS Model magnitude $r_{\rm Model}$ though it does not change the results since from a sample of 10000 galaxies within the magnitude/redshift range of our sample we find $r_{\rm Petro} \approx r_{\rm Model} +0.07$.

The adopted cosmology to estimate D_L is a flat Universe with the matter density parameter Ω_M=0.3 and cosmological constant Ω_Λ=0.7, with H_0=70 km s^{-1} Mpc^{-1}. The 'horizontal green histograms' in Fig. 2 show that the rate of detections of galaxies in the r-band become incomplete for sources with $M_r \gtrsim -21.0$ mag and $M_r \gtrsim -21.5$ mag in the redshift bins $0.02 \leqslant z \leqslant 0.1$ and $0.1 \leqslant z \leqslant 0.2$, respectively with almost double the number of detections in the higher redshift slice. Thus in the low-redshift Universe and within the current depth of H-ATLAS, most of the *Herschel* detections in the r-band consist of more luminous galaxies (and therefore those with larger stellar masses) which have lower values of $u - r$.

In order to analyze our sample in more detail, we divide galaxies into two populations by applying a cut on their $u - r$ colour indices. To find an optimum colour cut, a double-Gaussian function is fitted to the histogram for colour of all galaxies with $r_{\rm Petro} \lesssim 19.0$ mag. The combined function has a minimum around $u - r \approx 2.2$ mag. As such, from here on, unless otherwise stated, we refer to sources with $u - r \leqslant 2.2$ mag and $u - r > 2.2$ mag as *blue* and *red* objects, respectively.

In Fig. 3 we examine the differential fraction of detections of galaxies at 250μm as a function of r-band magnitude. We do this using $\sqrt{n}$ counting errors (n is the number of detected sources in each magnitude bin) for all optical sources (black histogram) as well as blue (blue dashed histogram) and red (red dash-dotted histogram) galaxies. The results, as presented in Fig. 3, show that (i) In general $\gtrsim 50$ per cent of SDSS galaxies with $r_{\rm Petro} \leqslant 17.0$ mag have 250μm counterparts in H-ATLAS. (ii) The submillimeter detection rate falls off rapidly as one moves toward fainter galaxies. This is mainly due to a decrease in the observed signal-to-noise ratio toward fainter galaxies. (iii) In each bin of r-band magnitude and for $r_{\rm Petro} \lesssim 18.0$ mag, the detection fraction is $\gtrsim 4$ times higher for 'blue' galaxies when compared to the 'red' population, indicating that the vast majority of detected sources are blue objects. Although such blue sources are in general star-forming galaxies, it does not mean that 250μm red detected objects are passive galaxies. We will discuss the properties of such sources in Section 3.3.

Finally in Table. 1 we present the total percentage of sources detected by H-ATLAS in samples of SDSS galaxies with differing limiting magnitudes. Samples of SDSS galaxies in the second column include galaxies with all colour indices, while those in the third and fourth columns contain blue and red objects, respectively.

3.2   Environment of detected sources

Our results in §3.1 show that submillimeter detected sources are preferentially blue sequence galaxies. Thus, since blue sequence galaxies are much more frequent in low density environments, we expect to find a lower detection rate in group/cluster environments than in the field.

To explore the environmental density of submillimeter detected galaxies, we consider the projected surface density, based on counting the number of nearest neighbours, i.e. the density within the distance to the Nth nearest neighbour. Although this is a 2D estimate, the redshift information of each galaxy is used to remove the background and foreground sources. The environmental density Σ_N around each galaxy detected at 250μm is determined from the following relation:

$$\Sigma_N({\rm Mpc}^{-2}) = \frac{N}{\pi d_N^2}, \qquad (2)$$

where d_N is the projected comoving distance to the $N^{\rm th}$ nearest neighbour that is within the allowed redshift range $\pm\Delta z c$=1000 km s^{-1} (Balogh et al. 2004a; Baldry et al. 2006). We set $N = 5$ in our analysis. The neighbouring galaxies are those with spectroscopic redshifts and $M_r \leqslant M_{\rm r,limit} - Q(z - z_0)$, where Q=1.6 is the evolution of the galaxy r-band luminosity relative to $z_0 = 0.1$, determined by Blanton et al. (2003). Horizontal histograms (grey thick lines) in the 'left' and 'right' panels of Fig. 2 show that galaxy counts become incomplete for the $M_r \gtrsim -19.0$ mag range if $0.02 \leqslant z \leqslant 0.1$ and $M_r \gtrsim$-20.5 mag if $0.1 \leqslant z \leqslant 0.2$. Thus the parameters ($M_{\rm r,limit}$,$z_0$) were set to $(-20.5, 0.1)$.

The rate of detection of the H-ATLAS sources as a function of the density parameter Σ_5 is plotted in panel 'a' of Fig. 4. Error bars are Poisson errors on the mean. Detection rates have been estimated for galaxies with $r_{\rm Petro} \leqslant 17.0$ mag, since galaxies with larger r-band magnitudes are not systematically detected due to their low signal-to-noise ratios. In other words, the majority of fainter galaxies are not detected in H-ATLAS, irrespective of their environments.

It is evident that the fraction of detected sources in low-density environments is larger by a factor of two in comparison to the rate of detection in high-density environments. This is expected, since the majority of detected objects in H-ATLAS are blue galaxies that preferentially populate the low-density regions. Results remain more or less the same if we use Σ_4 or Σ_6 instead of Σ_5, showing that the dependence of the detection rate on environmental density is not sensitive to the choice of N in Eq. 2. To obtain a better understanding of the type of detected objects that populate either low or high density environments, we plot the rate of detection of galaxies as a function of $r_{\rm Petro}$ for sources with different colours and densities in Fig. 4 (see panels 'b' and 'c').

The estimated projected density ranges from -2.0 to 2.0 on a logarithmic scale. We therefore define the threshold between low and high density environments at $\log \Sigma_5 \simeq 0$. As such, in panels 'b' and 'c' of Fig. 4, black histograms correspond to sources in low density environments with $\log(\Sigma_5/{\rm Mpc}^2) < 0$ while red dashed histograms refer to the fraction of detected galaxies in high density regions, i.e. $\log(\Sigma_5/{\rm Mpc}^2) \geqslant 0$. In addition, sources in panel 'b' have index $u - r \leqslant 2.2$ mag (e.g. blue objects) and the colour of those in panel 'c' is $u - r > 2.2$ mag (e.g. red objects). Although the number of blue galaxies is smaller in high-density regions, panel 'b' shows that the rate of detection remains the same in either environment. The situation is similar for the red galaxies, although the overall rate of detection of red objects is much smaller than for blue ones.

3.3   Nature of RED 250μm sources

We have already seen that the majority (~ 80 per cent) of galaxies detected in H-ATLAS at low redshift are blue galaxies while the rest ~ 20 per cent are red. However, such a fraction on red detected sources is an upper limit since many of these galaxies might have traces of recent star formation activities which is not reflected in their optical $u - r$ colour. In fact, UV-optical colours are more robust in classifying galaxies into blue/red categories in comparison to optical colours since they are more sensitive to recent star-formation activity (e.g. Schawinski et al. 2007; Cortese & Hughes 2009). The reason that we did not use UV-optical colour in Sec.3.1 is that for ~ 20 per cent of SDSS galaxies in the main sample, UV fluxes were not available from GAMA (see Sec.2.1). These galaxies (e.g. those without UV counterpart) are basically faint while
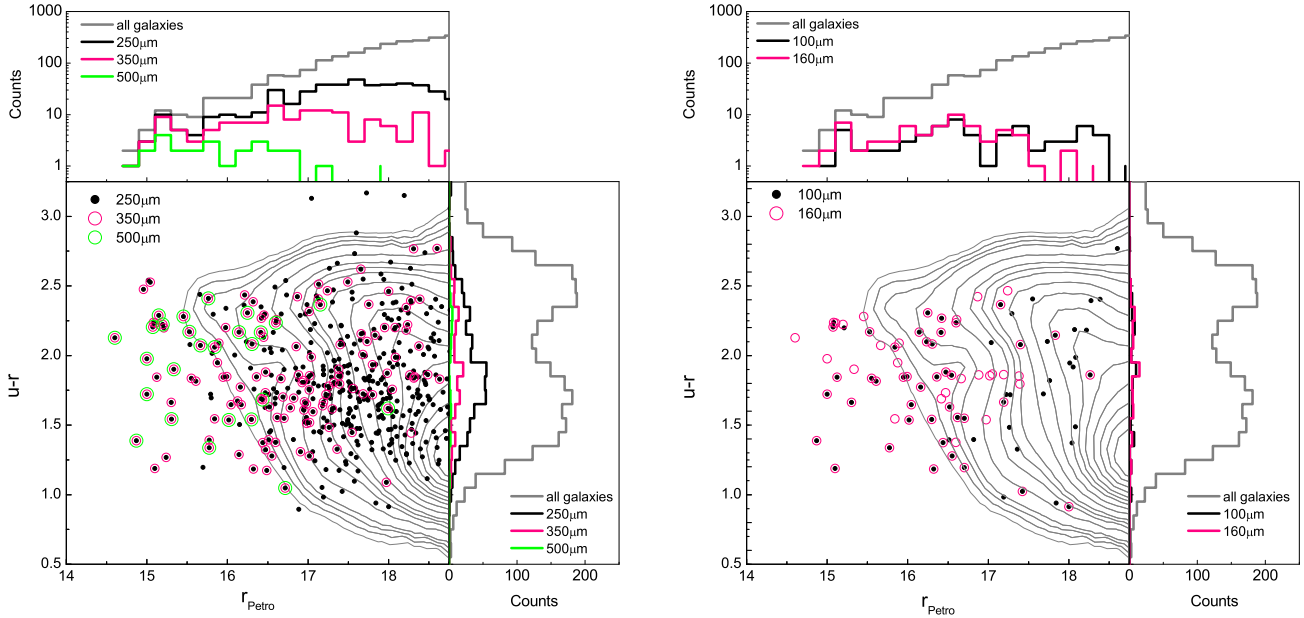
Figure 1. Colour-magnitude diagram of optically selected galaxies (grey contour lines) and their submillimeter counterparts with `Reliability` $\geqslant$0.8 detected at $\gtrsim 5\sigma$ by SPIRE (left panels) and PACS (right panel). Horizontal and vertical histograms show the distribution of galaxy optical colour ($u - r$) and r-band magnitude (r_{Petro}), respectively. Colours represent: 'grey' all galaxies; 'black' sources with SPIRE 250μm (left panel) and PACS 100μm (right panel) detections; 'pink' sources with SPIRE 350μm (left panel) and PACS 160μm (right panel) detections; 'green' sources with SPIRE 500μm detections.
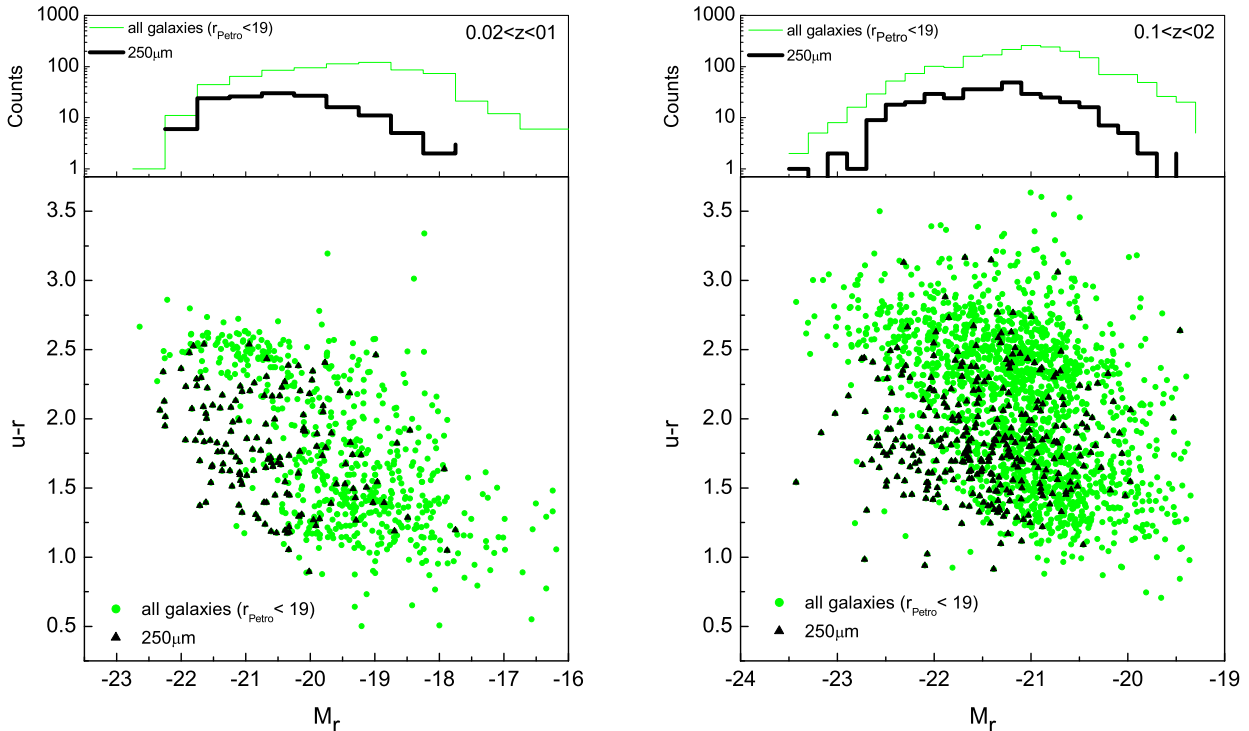
Figure 2. Same as in Fig. 1 but as a function of absolute r-band magnitude M_r and for 250μm detections. 'Left' and 'right' panels correspond to redshift bins $0.02 \leqslant z \leqslant 0.1$ and $0.1 \leqslant z \leqslant 0.2$, while horizontal histograms show the distribution of galaxy $u - r$ colour and absolute r-band magnitude, respectively. Colour of data-points/histograms represent: 'green' all galaxies; 'black' sources with SPIRE 250μm detections.
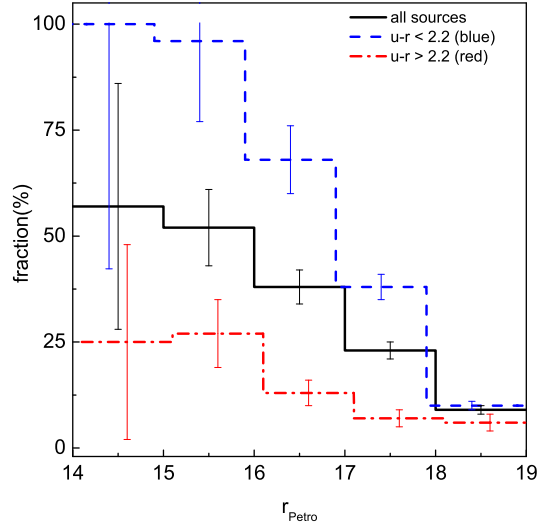
Figure 3. Histograms of the fraction of detected galaxies as a function of r-band magnitude. The black histogram includes all galaxies, while the two other histograms represent the detection rate of blue (blue dashed histogram; $u - r \leqslant 2.2$) and red (red dash-dotted histogram; $u - r > 2.2$) sources, respectively.

Table 1. The total fraction of sources detected by H-ATLAS among SDSS galaxies to differing limiting magnitudes, as shown in the first column. Samples of SDSS galaxies in the second column include galaxies with all colour indices, while those of third and forth columns contain blue and red objects, respectively.

sample limiting magnitude	Total fraction detected (percent)		
	all colours	blue $(u - r \leqslant 2.2$ mag)	red$(u - r > 2.2$ mag)
$r_{\mathrm{Petro}} \leqslant 16.0$ mag	53 ± 8	97 ± 18	27 ± 8
$r_{\mathrm{Petro}} \leqslant 17.0$ mag	42 ± 4	75 ± 7	17 ± 3
$r_{\mathrm{Petro}} \leqslant 18.0$ mag	29 ± 2	47 ± 3	11 ± 2
$r_{\mathrm{Petro}} \leqslant 19.0$ mag	17 ± 1	23 ± 2	9 ± 1
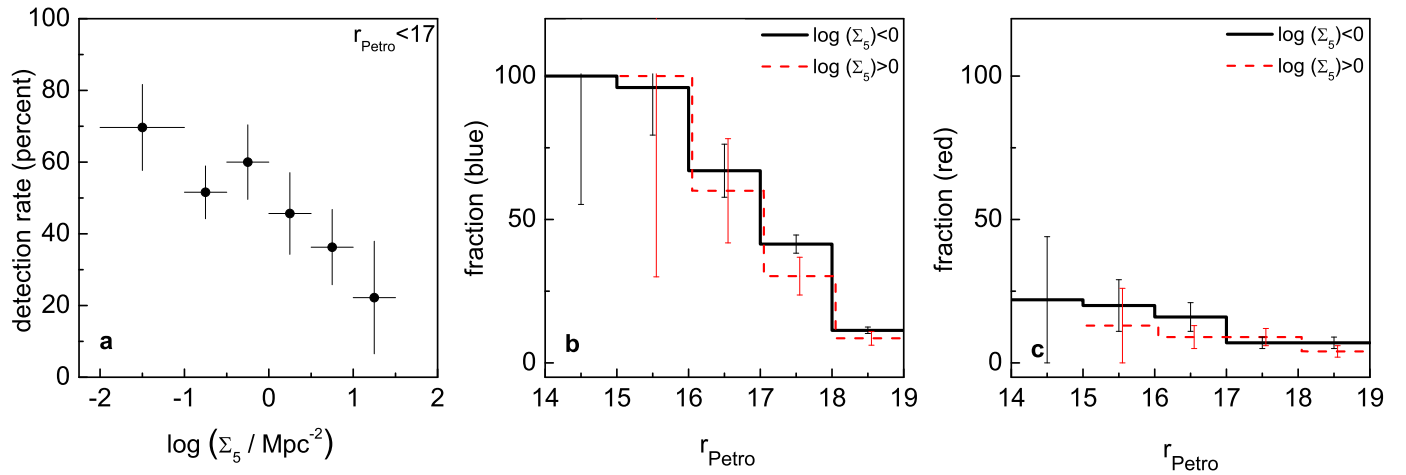
Figure 4. (a) The fraction of SDSS galaxies detected in H-ATLAS as a function of galaxy local density Σ_5 estimated using Eq. 2. **(b)** Histograms of the fraction of detected blue $(u - r \leqslant 2.2$ mag) galaxies as a function of r-band magnitude. 'The red dashed histogram' includes galaxies in high density regions $(\log(\Sigma_5/\mathrm{Mpc}^2) \geqslant 0)$ and 'the black histogram' includes those in low density regions $(\log(\Sigma_5/\mathrm{Mpc}^2) < 0)$. **(c)** Same as in 'b' but for red $(u - r > 2.2$ mag) galaxies.
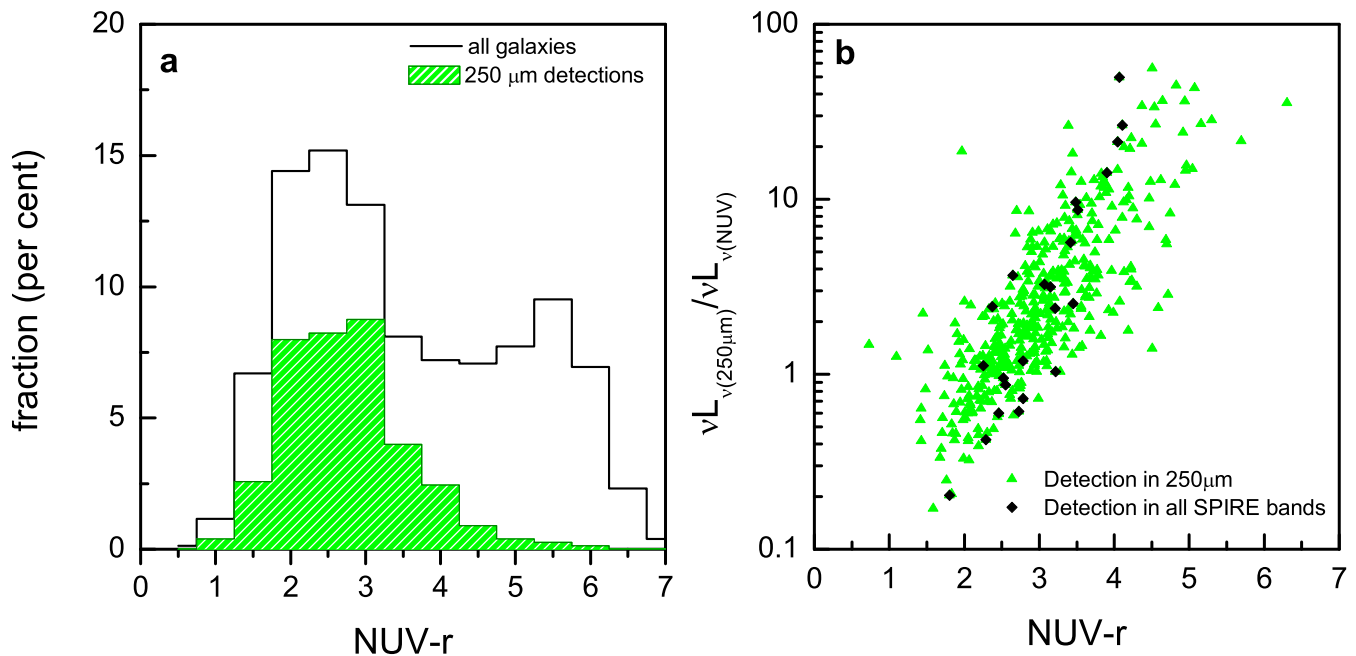
Figure 5. **(a)** NUV$-r$ colour distributions for all the SDSS galaxies (black histogram) with available UV fluxes as well as those detected in 250μm (green-shaded histogram).**(b)**The NUV$-r$ vs. $\nu L_{250}/\nu L_{\mathrm{NUV}}$ for galaxies with 250μm detections (green triangles). Overlaid (black diamonds) are galaxies detected in all SPIRE bands.

their optical colour distribution peaks around $u-r \approx 2.5$. So in order to avoid any biases in analyzing the fraction of source detection in previous sections, we were restricted to use the SDSS optical colours. Fortunately, NUV fluxes are available for $\gtrsim 98$ per cent of detected sources in 250μm which enable us to investigate the spectral properties of galaxies with 250μm detections from their UV-optical colours.

Thus in Fig. 5a, the NUV$-r$ colour distributions for all the SDSS galaxies with available UV fluxes (black histogram) as well as those detected in 250μm (green-shaded histogram) are shown. The black histogram in Fig. 5a shows a bimodality with a minimum around NUV$-r \approx 4.5$ mag found from fitting a double-Gaussian function to it. In addition, ~ 95 per cent of detected sources have NUV$-r \leqslant 4.5$ mag (i.e., blue in UV-optical colour) and just a small population of detected sources have NUV$-r \geqslant 4.5$ mag (i.e., red in UV-optical colour).

It is therefore interesting to know whether such red objects (i.e., NUV$-r \geqslant 4.5$ mag) are obscured star-forming systems or whether they are a population of quiescent/passive galaxies. As such, for all detected galaxies, a UV-optical vs. infrared colour-colour diagram is plotted in Fig. 5b, where green triangles represent sources detected at 250μm and highlighted data points (black diamonds) represent those H-ATLAS sources detected in all three SPIRE bands. Not surprisingly, the plot shows a correlation between NUV$-r$ and $\nu L_{250}/\nu L_{\mathrm{NUV}}$, with red galaxies having a higher $\nu L_{250}/\nu L_{\mathrm{NUV}}$ ratio than blue systems. A similar relation was found by Johnson et al. (2007) between the total far-infrared-to-near-ultraviolet luminosity ratio ($L_{\mathrm{TIR}}/L_{\mathrm{NUV}}$) and NUV$-r$ for a sample of local galaxies selected from SDSS.

By combining this relation with the library of infrared spectral energy distributions of Chary & Elbaz (2001), we can investigate the real nature of the H-ATLAS sources with NUV$-r >4.5$.

According to Chary & Elbaz (2001), the $\nu L_{250}/L_{\mathrm{TIR}}$ luminosity ratio varies in the range $\sim$4-65. Even assuming the lowest possible value (i.e., $\sim$4), this implies a $L_{\mathrm{TIR}}/L_{\mathrm{NUV}}$ ratio $\sim$6-250 for our red galaxies and we can use this value to estimate their NUV dust attenuation $A(NUV)$. If we adopt the typical relation between $L_{\mathrm{TIR}}/L_{\mathrm{NUV}}$ and $A(NUV)$ for star-forming objects (e.g. Buat et al. 2005), we find $A(NUV) \sim$1-4 mag. Interestingly, even using the relations between $L_{\mathrm{TIR}}/L_{\mathrm{NUV}}$ and $A(NUV)$ presented by Cortese et al. (2008) which take into account the heating of dust coming from evolved stellar populations, we still obtain $A(NUV) \geqslant$0.2-1.8[3].

Thus, this simple exercise shows that not surprisingly, the vast majority ($\geqslant$90 per cent) of the red objects detected by H-ATLAS in our sample have 'corrected' NUV$-r$ colour lower than 4.5 mag, i.e., they are red not because they are old/passive but mainly because they are obscured by dust. Of course, the presence (even if low in fraction) of a population of 'truly passive' systems in the H-ATLAS survey is a very intriguing possibility and might have important implications for our understanding of dust properties in galaxies. A detailed search for FIR emitting 'passive' systems and a discussion of their properties will be presented in a future work (Rowlands et al. 2011).

3.4 Variation of temperature with density

Our findings in Section 3.2 show that, irrespective of their environments, the rate of detection of submillimeter sources remains the

---

[3] These values have been obtained by using the most extreme case discussed by Cortese et al. (2008), i.e. $\tau < 2.8$, and they are thus lower limits to the real values for our sample.

same in either high or low density regions. Therefore it might be interesting to test whether the submillimeter properties (e.g., colours and dust temperature) of detected sources in H-ATLAS correlate with the environment.

Out of 71 galaxies with $\geqslant 3\sigma$ detections in all SPIRE bands, 38 have associated ($\geqslant 3\sigma$) PACS detections. To estimate the dust temperature of these 38 galaxies, we fit the submillimeter photometry with a single component modified black-body SED over the wavelength range 100–500μm. The equation for a single component black body is given by

$$F_\nu = \frac{\kappa_\nu}{D_{\rm L}^2} M B_\nu(T). \qquad (3)$$

Here M is the dust mass, T is the dust temperature, $B_\nu(T)$ is the Planck function, $D_{\rm L}$ is the luminosity distance to the galaxy, and κ_ν is the dust emissivity. The dust emissivity is assumed to be a power law in this spectral range, where $\kappa_\nu \propto \nu^\beta$. As we are not constraining dust masses, an absolute value of κ is not needed. We assume $\beta = 1.5$, though we note that the value is notoriously uncertain.

The uncertainties in the flux densities adopted from the standard H-ATLAS catalogue (e.g. Rigby et al. 2010) include the contribution from instrumental and confusion noise only. Thus we add the calibration errors of 10–20 per cent in the 100–160μm PACS bands and 15 per cent in all SPIRE bands in quadrature to those given in the H-ATLAS catalogue. The best-fit solution is found by minimizing the chi-squared (χ^2) function, yielding an average uncertainty in the fitting of ±1.8 K for temperature. The average reduced χ^2 value for all the fits is 0.7, with a standard deviation of 0.6. We find that the data in the 100–500μm range are accurately fitted by a single black-body component.

Fig. 6a shows that the submillimeter colour S_{100}/S_{500} correlates with the dust temperature. Such a correlation also exists between the dust temperature and other submillimeter colour indices, e.g., S_{160}/S_{350}, S_{250}/S_{500}, etc. However, not surprisingly, the relation between the S_{100}/S_{500} flux ratio and temperature is the strongest one. The estimated Spearman correlation coefficient in panel 'a' is $R_{\rm S} = 0.96$ and the best-fit linear regression to the data points (black dashed line) suggests the following relation for the dust temperature:

$$T(K) = 0.51(\pm0.02) \times S_{100}/S_{500} + 19.5(\pm0.3). \qquad (4)$$

A plot of the estimated dust temperature as a function of the density parameter Σ_5 for all galaxies in our sample is presented in panel 'b' of Fig. 6. Galaxies are divided into two subsamples based on their stellar mass content with circles and squares corresponding to sources with low ($9.5 \leqslant \log(M_*/h^{-2}M_\odot) \leqslant 10.5$) and high ($10.5 \leqslant \log(M_*/h^{-2}M_\odot) \leqslant 11.5$) stellar masses, respectively. Galaxy stellar masses, M_*, have been computed in units of solar mass from the relationship given by Yang et al. (2007) as follow:

$$\log(M_*/h^{-2}M_\odot) = -0.406 + 1.097(g-r) \\ -0.4(M_r - 5\log h - 4.64), \qquad (5)$$

using the $(g-r)$ colour and where M_r is the r-band absolute magnitude corrected for extinction and redshift. The green dashed line shows the mean temperature of the whole sample ($T \approx 25\pm4$ K)[4],

while green dotted lines indicate the standard deviation. This result fairly agrees with the rest-frame dust temperatures measured for a sample of the H-ATLAS galaxies studied in Dye at al. (2010) and Amblard et al. (2010) as well as those of the sample of BLAST sources determined by Dye at al. (2009). We note that the densities in panel 'b' of Fig. 6 span values typical of field galaxies and poor groups, whereas we are not able to trace very high density environments, such as compact groups or clusters of galaxies.

From inspection of Fig. 6b, it appears that the dust temperature does not show any systematic variation with the local density of either low mass or high mass galaxies. Further checks to see whether there is any correlation between either dust temperature or Σ_5 with other parameters such as galaxy redshift, physical size, and luminosity reveal none.

Interestingly, Fig. 6 shows the presence of six outliers (marked as 'A' to 'F') characterized by dust temperatures ($T \approx 32 \pm 2$ K) significantly higher than the values typically observed in the rest of our sample. SDSS images (see Fig. 7) reveal the presence of diffuse tidal stellar features associated with at least three (A, C and F) of the six outliers in Fig. 6. These are the only galaxies in our sample of 38 objects with obvious signatures of tidal disturbance, suggesting that the dust temperature has recently been enhanced via gravitational interaction.

4   CONCLUSIONS

This study presents a variety of statistics based on *Herschel* observations acquired during the H-ATLAS Science Demonstration Phase. We started with a sample of SDSS-GAMA galaxies at low redshift ($0.02 \lesssim z \lesssim 0.2$) and then characterized the properties of the matched submillimeter sources detected in the H-ATLAS survey from their colours. Our results can be summarized as follows:

• At least ≈ 50 per cent of all SDSS galaxies with $r_{\rm Petro} \lesssim 17.0$ mag are detectable in H-ATLAS. In addition, the vast majority of detected sources in H-ATLAS are blue/star-forming objects. The majority of undetected faint/blue sources with $r_{\rm Petro} > 17.0$ mag remain undetected due to their lower signal-to-noise. By using the NUV$-r$ index as a proxy for galaxy colour, we detect a small fraction (~ 5 per cent) of red objects (NUV$-r > 4.5$ mag) which are mainly galaxies with a higher level of dust attenuation. As such the red sequence population which is dominated by less-dusty/passive objects, do not seem to have a significant contribution to the observed submillimeter emission in red objects.

• The rate of detection of galaxies decreases from ≈ 70 per cent to 30 per cent as one moves from low density to high density regions. This is due to the fact that low density regions are more populated by blue/dusty objects. However the detection rate of blue/red galaxies remains constant in either low or high density environments. In other words the colour of an object rather than its local density determines whether it is detectable in H-ATLAS.

• The estimated dust temperature in galaxies with detections in all SPIRE bands and $\geqslant 3\sigma$ detections in PACS bands is 25 ± 4 K, regardless of the environment. However, we show that gravitationally perturbed systems have temperatures significantly higher than the rest of our sample.

The next crucial step is to extend our analysis to a wider range of galaxy densities/stellar-masses to see how far the environment of galaxies could affect their observed submillimeter properties. While *Herschel* observations of the Virgo cluster are starting to

---

[4] The estimated mean temperature is $T_{mean} \approx 22 \pm 4$ K in the case of $\beta = 2.0$. In fact our data show a strong correlation ($R_{\rm S} = 0.99$) between the estimated temperatures based on either values of β such that $T_{\beta=2.0} = 0.78(\pm0.01) \times T_{\beta=1.5} + 2.1(\pm0.2)$.
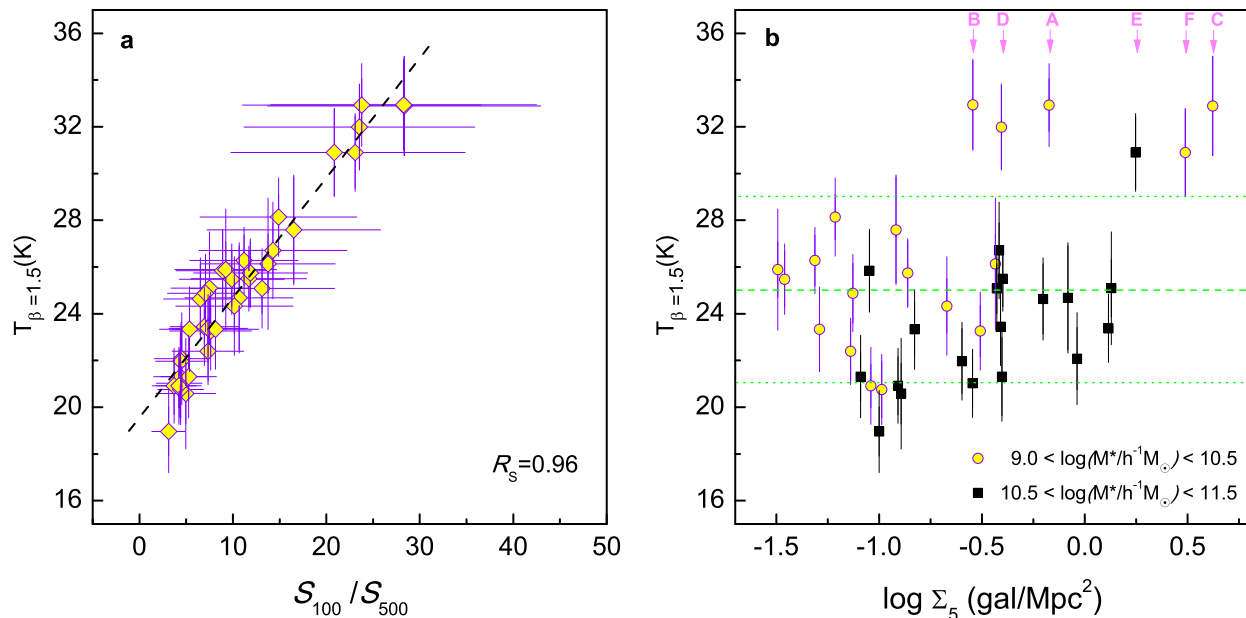
Figure 6. (a) Dust temperature vs. submillimeter colour S_{100}/S_{500}. The dashed line shows the linear regression fit as described by Eq. 4. **(b)** Dust temperature as a function of the local density of galaxies, Σ_5, for sources with $\geqslant 3\sigma$ detections in SPIRE/PACS bands. The green dashed line intersects the y-axis at the mean temperature of the whole sample ($T \approx 25$ K) while green dotted lines represent the standard deviation of the mean temperature. Circles and squares represent galaxies with low ($9.5 \leqslant \log(M_*/h^{-2}M_\odot) \leqslant 10.5$) and high ($10.5 \leqslant \log(M_*/h^{-2}M_\odot) \leqslant 11.5$) stellar mass, respectively. The SDSS images of objects marked as 'A' to 'F' (with 'A' having the maximum temperature) are shown in Fig. 7.
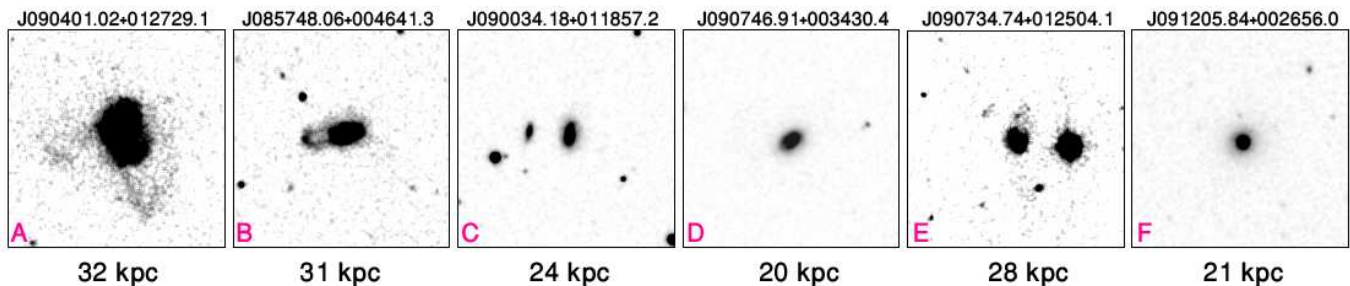
Figure 7. SDSS postage stamp images in the r-band (70×70 arcsec^2) of galaxies corresponding to the marked data points in Fig. 6. Images are sorted (left-to-right) according to the estimated dust temperature. The SDSS optical major isophotal diameter in the r-band (e.g. `isoA-r`) has been used to measure the optical linear diameter of each galaxy D_{25} in units of kpc as indicated on each panel.

reveal how the environment can affect the dust properties of cluster galaxies (Cortese et al. 2010), only a wide-area survey like H-ATLAS will make it possible to unveil the effects of nurture across the whole range of densities (from voids to the cores of clusters). Thus, once completed, the H-ATLAS survey together with data from the GAMA survey will offer a unique data set, spanning from the UV to the submm, with which to investigate the star formation history of galaxies over a large range of galaxy densities/stellar-masses. At the same time, properties such as dust temperature and dust-mass/stellar-mass of galaxies can be explored as a function of environment using PACS/SPIRE submillimeter fluxes. This will enable us to further investigate the correlation between star formation history and dust properties of galaxies as a function of stellar mass and local density.

REFERENCES

Abazajian, K.N. et al., 2009, ApJS, 182, 543

Amblard, A., et al. 2010, A&A, 518, L9

Baldry, I. K., Balogh, M. L., Bower, R. G., Glazebrook, K., Nichol, R. C., Bamford, S. P., & Budavari, T. 2006, MNRAS, 373, 469

Baldry, I. K. et al., 2004, ApJ, 600, 681

Ball, N. M., Loveday, J., Brunner, R. J., 2008, MNRAS, 383, 907

Balogh et al., 2004, MNRAS, 348, 1355

Balogh et al., 2004, ApJL, 615, 101

Blanton et al., 2003, ApJ, 592, 819

Blanton et al., 2005, ApJ, 629, 143

Buat, V., Xu, C., 1996, A&A, 306, 61

Buat et al. 2005, ApJ, 619, L51

Chary, R., Elbaz, D., 2001, ApJ, 556, 562

Chilingarian, I., Melchior, A., Zolotukhin, I., 2010, MNRAS, 405, 1409

Colless, M. at al., 2001, MNRAS, 328, 1039

Cortese, L. et al., 2008, MNRAS, 386, 11684

Cortese, L. & Hughes T. M., 2009, MNRAS, 400, 1225

Cortese, L. et al., 2010, A&A, 518, L49

Devlin, M. et al. 2009, Nature, 458, 737

Dressler, A., 1980, ApJ, 236, 351

Driver, S. et al., 2007, MNRAS, 379, 1022

Driver, S.P. et al., 2010, MNRAS, 413,971

Dunne, L., &; Eales, S., 2001, MNRAS, 327, 697

Dye, S., Ade, P. A. R., Bock, J. J., et al. 2009, ApJ, 703, 285

Dye, S. et al. 2010, A&A, 518, L10

Eales, S. et al., 2010, PASP, 122, 499

Gomez, P. L., 2003, ApJ, 584, 210

Griffin, M. et al., 2007, Advances in Space Research, 40, 612

Hill, D.T., Driver, S.P., Cameron, E., Cross, N.,Liske, J., Robotham, A., 2010, MNRAS, 404, 1215

Hill, D.T. et al., 2011, MNRAS, 412, 765

Ibar, E. et al., 2010 (arXiv:1009.0262)

Johnson, B. D. et al., 2006, ApJ, 644, 109

Johnson, B. D. et al., 2007, AJSS, 173, 377

Lee, J.H., Lee, M.G., Park, C., Choi, Y-Y., 2010, MNRAS, 403, 1930

Lewis, I. et al., 2002, MNRAS, 334, 673

O'Mill, A. L., Padilla, N., Lambas, D. G., 2008, MNRAS, 389, 1763

Park, C. et al., 2007, ApJ, 658, 898

Pascale, E., Ade, P. A. R. , Bock, J. J., Chapin, E. L., Chung, J. et al., 2008, ApJ, 681, 400

Pascale, E. et al., 2010 (submitted to MNRAS)

Petrosian, V., 1976, ApJ, 209, 1

Pilbratt G. et al., 2010, A&A, 518, 1

Poglitsch, A. et al., 2006, SPIE, 6265, 8

Popescu, C. C.; Tuffs, R. J., Völk, H. J., Pierini, D., Madore, B. F., 2002, ApJ, 567, 221

Rigby, E. et al., 2010 (submitted to MNRAS)

Robotham, A. et al., 2010, PASA, 27, 76

Rowlands, K., Dunne, L., Maddox, S. et al., 2011, in preparation

Schawinski, K., Kaviraj, S., Khochfar, S. et al., AJSS, 2007, 173, 512

Seibert, M. et al. (in preparation)

Smith, D.J.B. et al., 2010 (arXiv: 1007.5260)

Strateva, I. et al., 2001, AJ, 122, 1861

Sutherland, W., Saunders, W., 1992, MNRSA, 259, 413

Tojeiro, R., Wilkins, S., Heavens, A. F., Panter, B., Jimenez, R.,2009, ApJS, 185, 1

Tuffs, R. J., Popescu, C. C., Pierini, D., Völk, H. J., Hippelein, H., Leech, K., Metcalfe, L., Heinrichsen, I., Xu, C., 2002, ApJS, 139, 37

Vlahakis, C., Dunne, L., Eales, S., 2005, MNRAS, 364, 1253

Wyder T. K. et al., 2007, AJSS, 173,293

Yang X., Mo H.J., van den Bosch F.C., Pasquali A., Li C., Barden M., 2007, ApJ, 671, 153